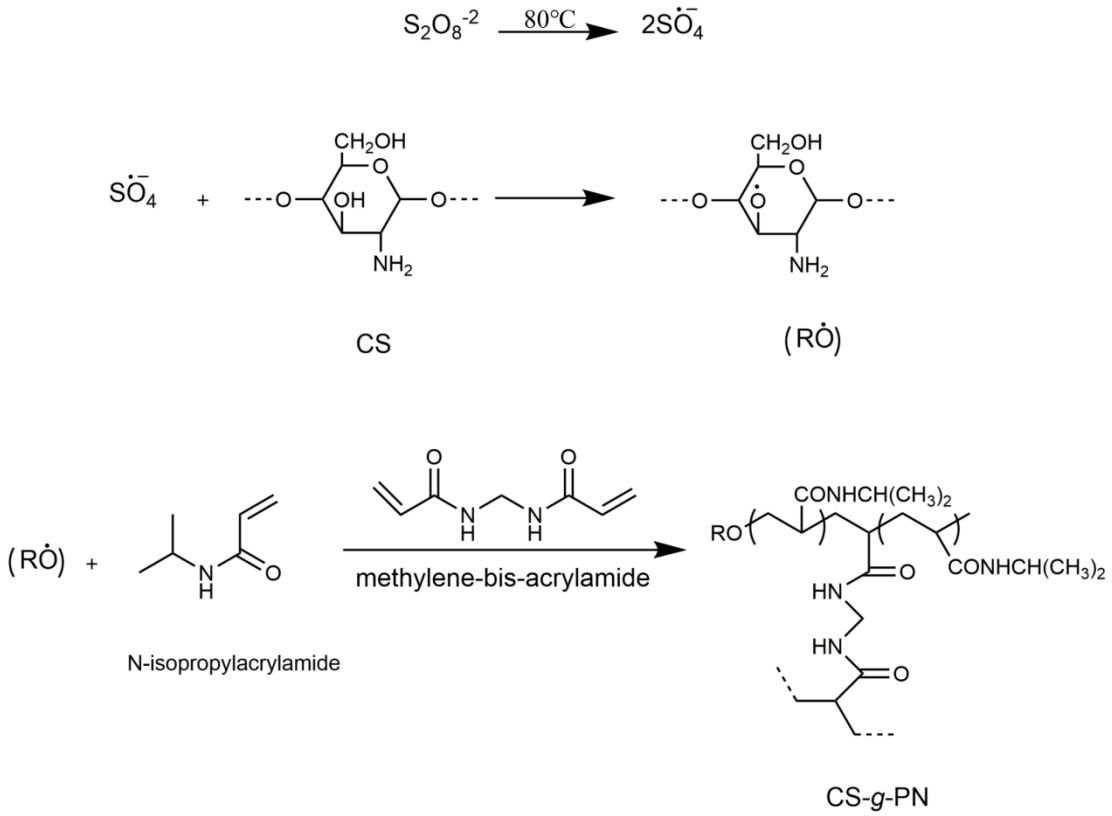

Figure S1. Schematic synthesis of CS–*g*–PN.

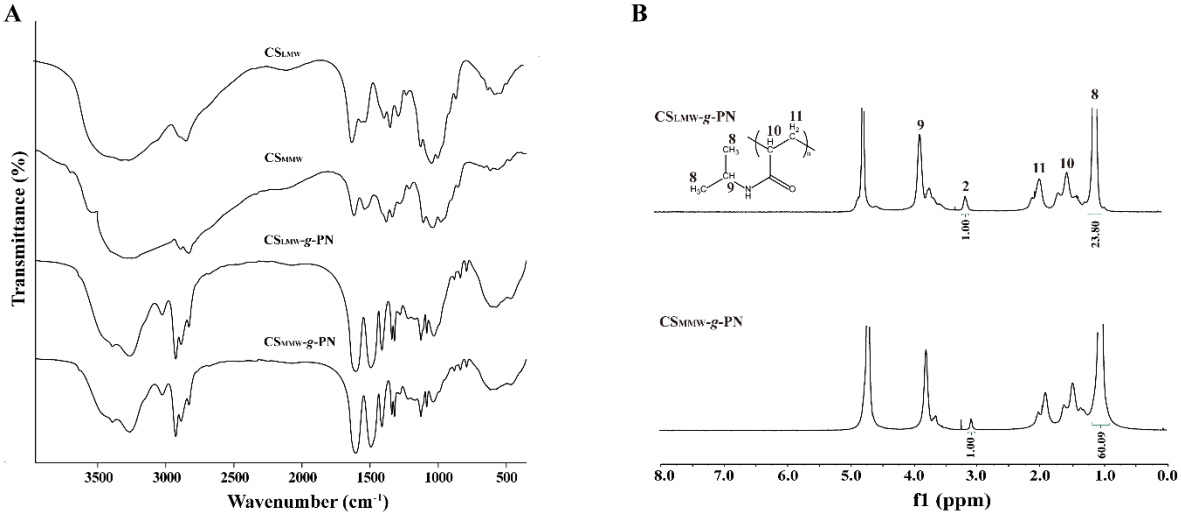

Figure S2. Characterization of CS–*g*–PN. (A) FT–IR spectrum of CSLMW, CSMMW, CSLMW–*g*–PN and CSMMW–*g*–PN. (B) ^{1}H–NMR spectrum of CSLMW–*g*–PN and CSMMW–*g*–PN.

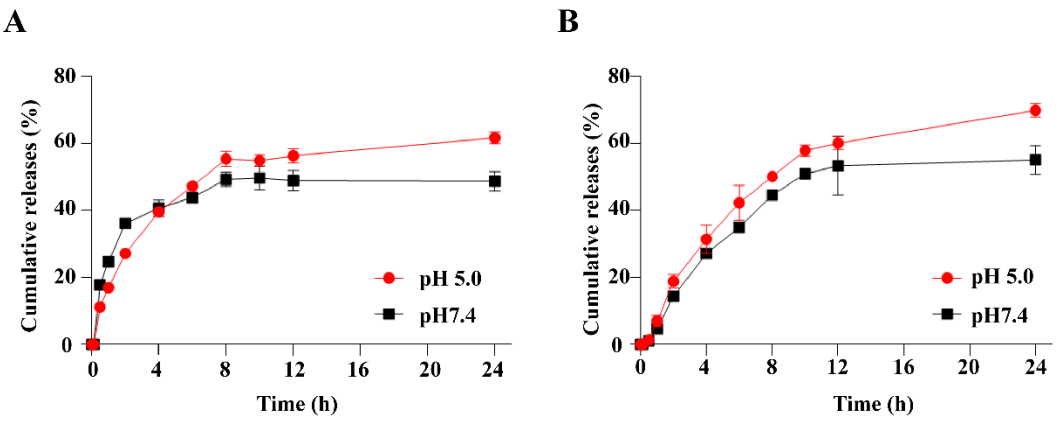

Figure S3. In vitro release profile of CUR@CS–NP. (A) CUR@CS$_{LMW}$–NP (B) CUR@CS$_{MMW}$–NP.

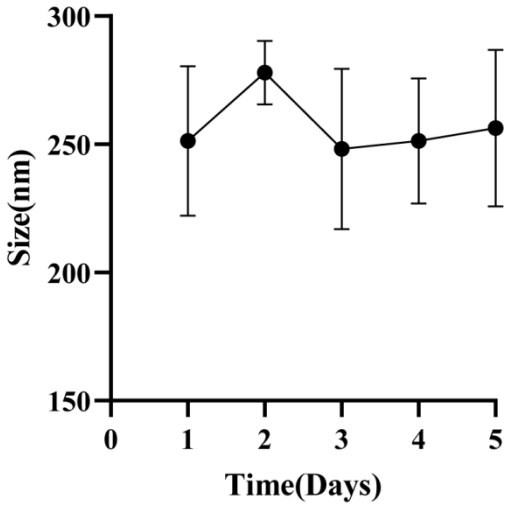

Figure S4. Colloidal stability of CUR@CS–NP@HA within 5days.

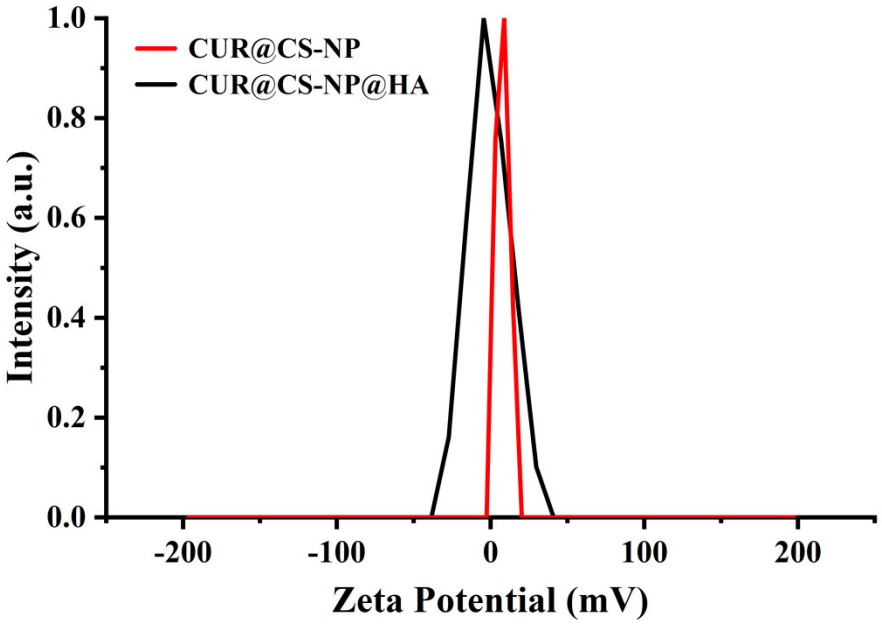

Figure S5. Zeta Potential distributions of CUR@CS−NP and CUR@CS−NP@HA.

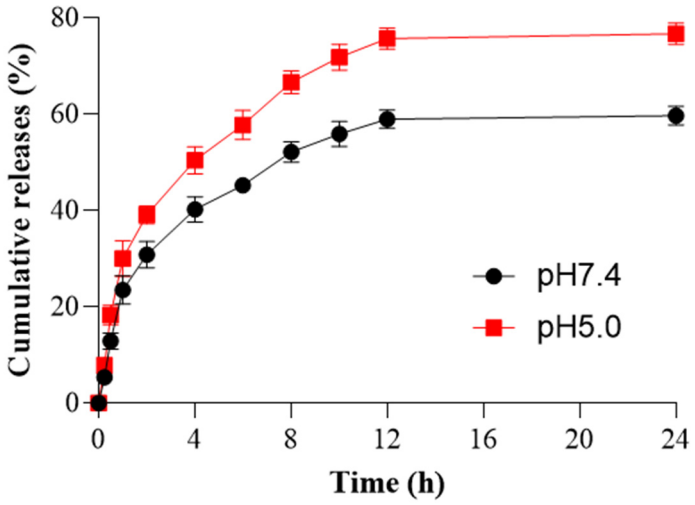

Figure S6. In vitro release profile of CUR@CS–NP@HA.

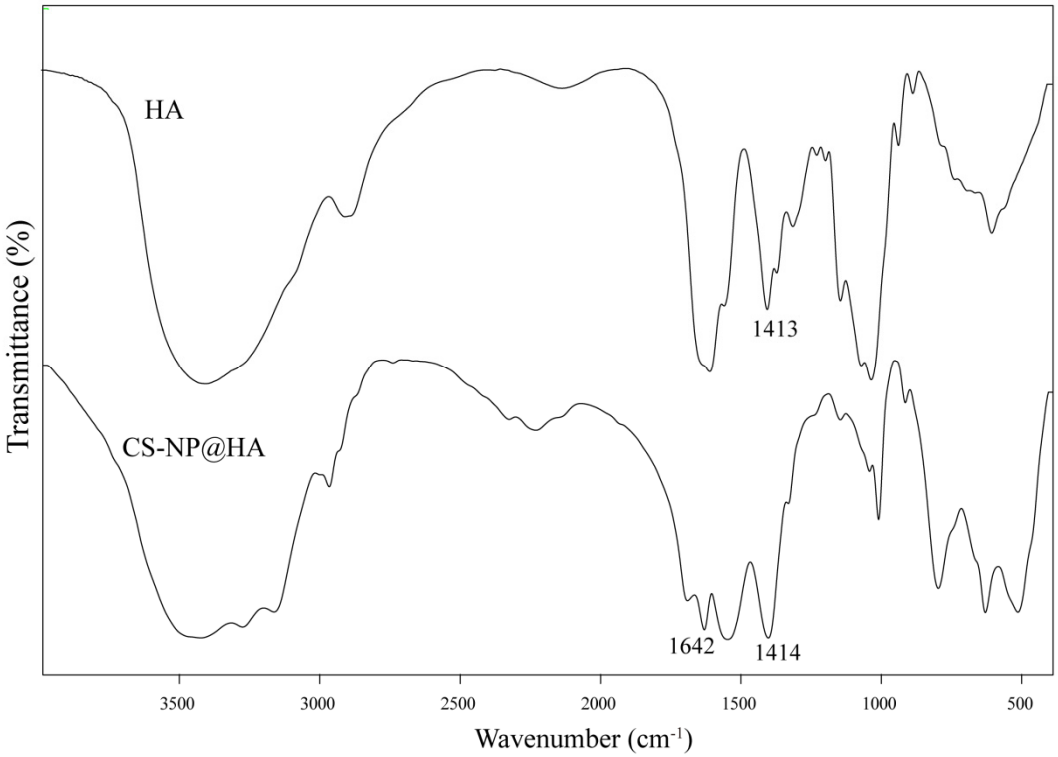

Figure S7. FT−IR spectra of HA and CS−NP@HA. Different from FT−IR spectrum of CS−*g*−PN, the amide bond absorption peak of CS at CS−NP@HA shifts to 1642 cm^{-1}, and the C=O (−COOH) symmetric stretching vibration peak of HA shifts from 1413 cm^{-1} to 1414 cm^{-1}, all of which indicates HA interacting with CS−*g*−PN.

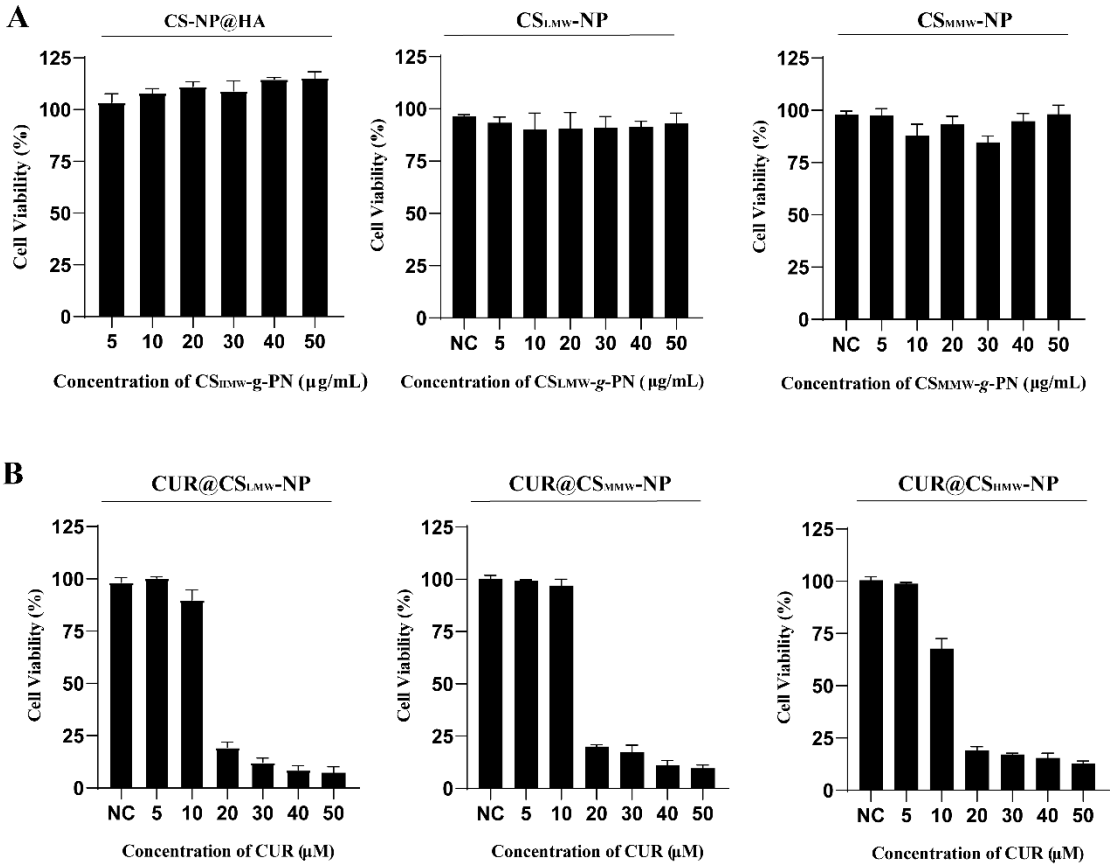

Figure S8. Cell cytotoxicity assay. (A) Cytotoxicity of blank NPs. (B)Cytotoxicity of CUR@CS$_{LMW}$−NP, CUR@CS$_{MMW}$−NP and CUR@CS$_{HMW}$−NP.

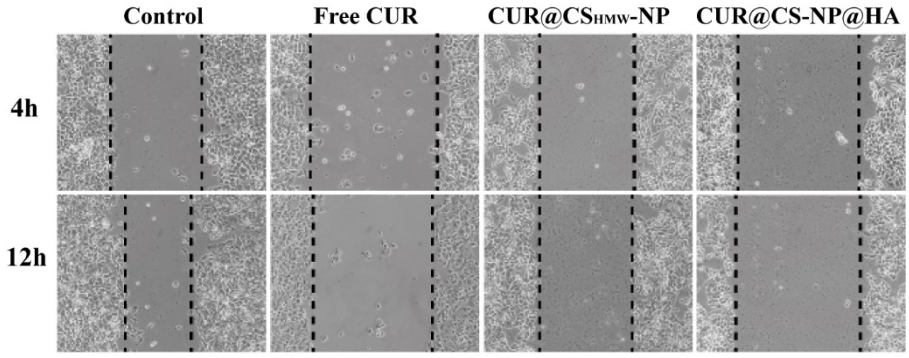

Figure S9. The migration of 4T1 cells treated with NPs in 4h and 12h.

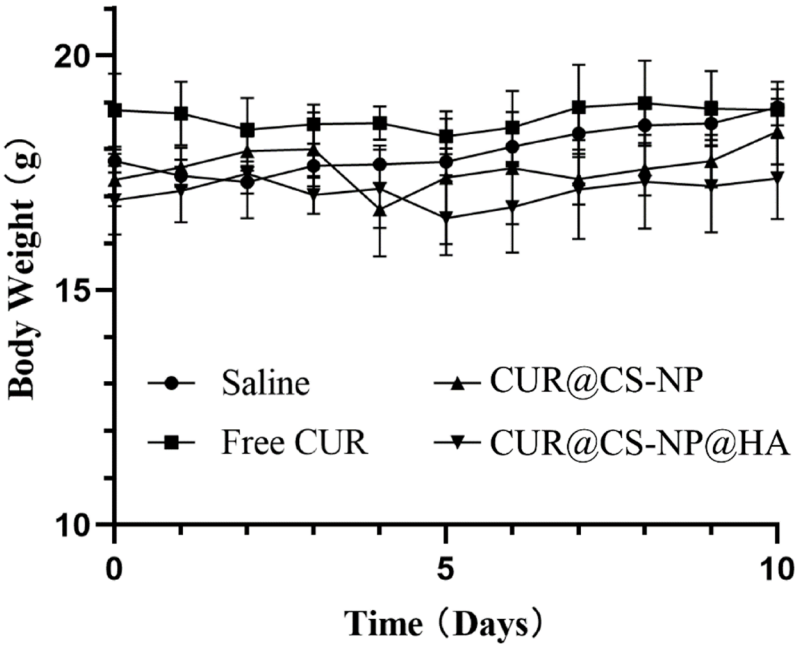

Figure S10. Body weight change in Balb/c mice over 10 days.

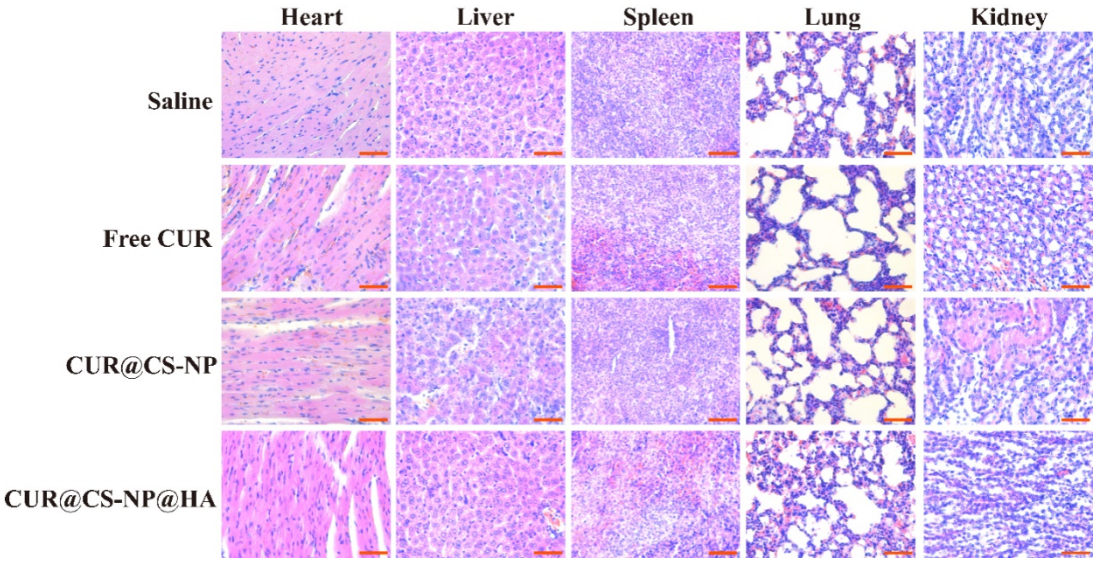

Figure S11. After 10 days of treatment, HE staining of heart, liver, spleen, lung and kidney tissues were taken from tumor−bearing Balb/c mice (scale bar=51μm).